POLITECNICO
MILANO 1863

DIPARTIMENTO DI
SCIENZE E TECNOLOGIE
AEROSPAZIALI

Department of Aerospace Science and Technology

Space Propulsion course (A.Y. 2021/22)

Final Workshop:

Liquid Propulsion System: Analysis and Design

Professor Filippo Maggi

Group: Discovery One

Alessandro Cambielli	10619322
Giovanni Cappellari	10668116
Lorenzo Casoni	10609874
Luca Cederle	10618136
Alessia Lancini	10668620
Davide Lanza	10567211
Rocco Larocca	10660565
Matteo Mascelloni	10324919
Afaq Shakeel	10625777

Abstract

Liquid propellant systems provide a wide range of fuel/oxidizer combinations: MICIOBAU Propulsion Company has selected a bi-propellant system with Hydrogen Peroxide (H_2O_2 at 87.5%) and an highly refined form of Kerosene (*RP-1*).

The aim of this paper is to design and to analyze the performances of a 100 N thrust propulsion unit characterized by the propellant discussed above and to study the main propulsion parameters during the firing as a function of time. Simultaneously, a critical analysis from the manufacturing viewpoint will be provided, focusing on materials and production technologies, hence identifying their operational advantages or limitations in terms of thermo-structural resistances and uncertanties. Finally, a qualitative sizing for a down/up-scaling of the obtained technology will be performed assigning a 10 or a 1000 N thrust.

Nomenclature and Constants

Physical Quantities:

Γ	Vandenkerckhove function	$[-]$	r	Oxidizer to fuel ratio	$[-]$
c_f	Thrust coefficent	$[-]$	γ	Ratio of specific heats	$[-]$
p	Pressure	$[Pa]$	R	Specific gas constant	$[\frac{J}{kg \cdot K}]$
μ	Viscosity	$[Pa \cdot s]$	T	Tempertaure	$[K]$
V	Volume	$[m^3]$	v	Velocity	$[m/s]$
$\mathscr{F}$	Thrust	$[N]$	$\dot{m_p}$	Propellant mass flow rate	$[kg/s]$
ρ	Density	$[kg/m^3]$	C^*	Characteristic Velocity	$[m/s]$
c_p	Isobaric specific heat	$[\frac{J}{kg \cdot K}]$	c_v	Isochoric specific heat	$[\frac{J}{kg \cdot K}]$
I_{tot}	Total impulse	$[N \cdot s]$	I_{sp}	Gravimetric specific impulse	$[s]$
M	Mach number	$[-]$	t_b	Burning time	$[s]$
λ	Correction factor	$[-]$	ε	Expansion ratio	$[-]$
g_0	Gravity acceleration	$[m/s^2]$	A_e	Exit area	$[m^2]$
α	Nozzle divergent half angle	$[deg]$	β	Nozzle convergent half angle	$[deg]$
L^*	Characteristic length	$[m]$	d_{inj}	Injection diameter	$[mm]$
Re	Reynolds number	$[-]$	K	Feeding lines losses	$[\frac{1}{m \cdot kg}]$
c_d	Discharge coefficient	$[-]$	m	Mass	$[kg]$

Acronyms:

CEA	Chemical Equilibrium for Applications	LRE	Liquid Rocket Engine
O/F	Oxidizer to Fuel Ratio	ALM	Additive Layer Manufacturing

Constants:

g_0	9.81 m/s^2	t_b	100 s
ρ_{H2O2}	1414 kg/m^3	ρ_{RP-1}	810 kg/m^3
ρ_{H2O}	1000 kg/m^3	ε	80
μ_{H2O2}	$1.249 \cdot 10^{-3} Pa \cdot$s	μ_{RP-1}	$1.58 \cdot 10^{-3} Pa \cdot$s

Contents

List of Figures

List of Tables

Chapter 1

Introduction

1.1 Liquid Rocket Engines: an Overview on the System

Liquid Rocket Engines (LRE) represent one of the main propulsion technologies available in space field, guaranteeing high performances, safety and a state of the art solution.
For this paper, a bi-propellant liquid propulsion system (Fig. 1.1) has been chosen, providing a blow-down architecture, a liquid injection and pure regenerative cooling system. The purpose of this first point is to give an overview of such similar systems, focusing on the propulsive-parameter trends during injection and combustion.
Concerning the choice of propellant combination for these types of rockets, H_2O_2 with kerosene represents a relatively high density propellant couple yielding reasonable specific impulse. Unlike other storable propellant pairs it is a non-toxic, green propellant. However, Hydrogen Peroxide becomes unstable at temperatures greater than 414 K and decomposes at 1% per year rate requiring a further care in its handling. The propellant combination assigned for this paper is RP-1 (fuel) and Hydrogen Peroxide at 87.5% weight concentration with water at 12.5% (oxidizer).

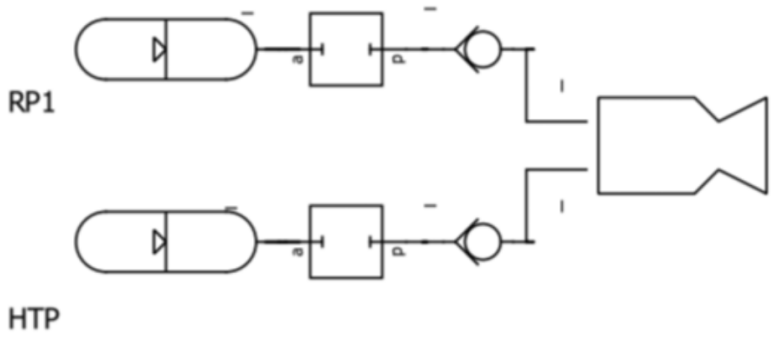

Figure 1.1: Scheme of the Propulsion System

1.2 Additive Manufacturing for LRE Solutions

Injector and combustion chamber correspond to two of the most critical components of a LRE from a thermo-structural point of view: their production requires high accuracy and machinability, guaranteeing at the same time an adequate production capability.
Therefore, metal additive layer manufacturing (ALM) appears very appealing, since it could reduce hardware cost, allow shorter fabrication schedules, increase reliability and performances [7].

Inconel alloy 718 is a high-strength, corrosion-resistant nickel chromium material used from 20 K to 1033 K: its good tensile, fatigue, creep, and rupture strength lead to a wide range of applications [10].
Since Inconel 718 is fixed by the assignment requirements, three main limits in terms of material property shall be considered for the injection plate and the combustion chamber design:

- Porosity appears to be higher after ALM production, affecting negatively the components with passing holes between internal and external parts;
- Roughness of surfaces results much higher, affecting negatively the fluid pressure losses especially in high kinetic energy components;
- Inconel shows its best performances up to a temperature of 1033 K: high strength at greater temperatures could be developed by precipitation heat treatments with aging, but for a combustion chamber (in which operational temperatures are well above 2000 K) excellent regenerative cooling will be required.

Good accuracy requirements combined with high production rate for ALM has led to the selection of ProMaker P1000 X SLS 3D Printer by ProdWays Tech as the main manufacturing tool [8]. The machine is characterized by a build chamber size of 300x300x360 mm, it has a built rate of 2 liters/hour and highly accurate tolerances (± 0.05 mm).

Chapter 2

Nominal Design

2.1 Performance Parameters Determination

The combustion problem, followed by an isentropic expansion through the rocket, is evaluated through NASA CEA: thus, thermodynamic performance parameters based on a frozen hypothesis at combustion level can be effectively determined. The O/F has been set to 6, a sub-optimal value in terms of specific impulse, in order to have more optimal condition during the motor time evolution. As a matter of fact, during the firing the O/F tends to increase. Starting from a higher and more optimal value of O/F would have resulted in higher performances at the start of the operations, but in a fast degradation in the subsequent times.

Table 2.1: CEA Output in nominal conditions

Combustion chamber temperature T_c	Specific gas constant R	Ratio of specific heats γ
2545.3 K	401.89 $J/(kg \cdot K)$	1.187

As a design constraint it is requested to guarantee an expansion ratio ε of 80 and a nominal combustion chamber pressure p_c of 20 bar. Another constraint is to ensure that the thrust value never decays below the 50% of the nominal value, which has been set to $T = 100\,N$,
The inverse of the expansion area ratio can be written as:

$$\frac{1}{\varepsilon} = \left(\frac{\gamma+1}{2}\right)^{\frac{1}{\gamma-1}} \left(\frac{p_e}{p_c}\right)^{\frac{1}{\gamma}} \sqrt{\frac{\gamma+1}{\gamma-1}\left[1-\left(\frac{p_e}{p_c}\right)^{\frac{\gamma-1}{\gamma}}\right]} \tag{2.1}$$

and solving the equation for the pressure ratio with `fzero` eventually yields $p_e = 0.001 p_c$.
At this point, the performance of the combustion chamber can be evaluated through the following parameters:

$$\Gamma = \sqrt{\gamma\left(\frac{2}{\gamma+1}\right)^{\frac{\gamma+1}{\gamma-1}}} = 0.6463 \tag{2.2}$$

$$C^* = \frac{\sqrt{RT_c}}{\Gamma} = 1564.9\,m/s \tag{2.3}$$

And then the exit velocity as follows:

$$v_e = \sqrt{1-\left(\frac{p_e}{p_c}\right)^{\frac{\gamma-1}{\gamma}}} \sqrt{\frac{2\gamma}{\gamma-1} R \cdot T_c} = 2940.2\,m/s \tag{2.4}$$

The thrust coefficient and the specific impulse are computed considering vacuum expansion ($p_a = 0$) and the divergence thrust loss coefficient λ_N[1], from the following equations:

$$c_F = \lambda_N \Gamma \sqrt{\frac{2\gamma}{\gamma - 1}} \sqrt{1 - \left(\frac{p_e}{p_c}\right)^{\frac{\gamma-1}{\gamma}}} + \frac{p_e - p_a}{p_c}\varepsilon = 1.9201 \tag{2.5}$$

$$I_s = \frac{c_F C^*}{g_0} = 306.29\ s \tag{2.6}$$

2.2 Nozzle and Combustion Chamber Design

The throat and exit areas are found by exploiting the following relations:

$$A_t = \frac{\mathscr{F}}{p_c c_F} = 26.04 \cdot 10^{-6}\ m^2 \quad A_e = \varepsilon A_t = 20.83 \cdot 10^{-4}\ m^2 \tag{2.7}$$

With the nominal O/F equal to 6, the mass flow rate is computed as:

$$\dot{m}_p = \frac{P_c A_t}{C^*} = 33.28 \cdot 10^{-3}\ kg/s \Rightarrow \begin{cases} \dot{m}_{ox} = \frac{O/F}{1+O/F}\dot{m}_p = 28.52 \cdot 10^{-3}\ kg/s \\ \dot{m}_{fu} = \dot{m}_p - \dot{m}_{ox} = 4.75 \cdot 10^{-3}\ kg/s \end{cases} \tag{2.8}$$

For simplicity, a conical nozzle has been chosen and its divergence and convergence half angles have been selected from literature as equal to $\alpha = 15\,deg$ and $\beta = 40\,deg$ [1]. From the equations reported in Appendix 4.1, a geometrical sizing of the nozzle has been carried out. The results are available in Table 2.2:

Table 2.2: Geometrical characterization of the nozzle

External radius r_e	Throat radius r_t	Divergence length	Convergence length
25.75 mm	2.88 mm	85.36 mm	4.95 mm

After the geometrical sizing of the nozzle it has been possible to compute the geometry of the combustion chamber imposing a $Ma = 0.1$. A lower Mach number compared to a more typical 0.2-0.3 range increases the dimensions of the section of the combustion chamber and, in this case, improves its manufacturability. A cylindrical shape has been selected, since it guarantees the absence of edges, reducing the possibility of failure due to high pressure in the chamber. As an hypothesis, the characteristic length L^* has been imposed equal to 1.78: this value corresponds to the maximum one indicated by Table 5.6 of [3] since larger residence times are expected due to liquid injection of the propellants in the combustion chamber lack of a catalyst. The obtained data are available in Table 2.3.

Table 2.3: Geometrical characterization of the combustion chamber

Contraction ratio ε_c	Area A_c	Radius r_c	Length L_c
5.9607	155.22 mm^2	7.03 mm	298.29 mm

[1] $\lambda_N = \frac{1}{2} \cdot (1 + cos\alpha)$

2.3 Injection plate design

In order to compute the number of injectors needed and their respective diameter the fuel and oxidizer values must be known. The oxidizer density, considering its mass concentration at 87.5% with the remaining part composed of water, is computed using the following formula:

$$\rho_{ox} = \frac{100}{\frac{87.5}{\rho_{H2O2}} + \frac{12.5}{\rho_{H2O}}} = 1344 \, \frac{kg}{m^3} \tag{2.9}$$

A standard injector from Sutton Tables [4], in particular the short tube with conical entrance type characterised by $d_{inj} = 10^{-3}\, m$ and $c_d = 0.82$, has been selected.

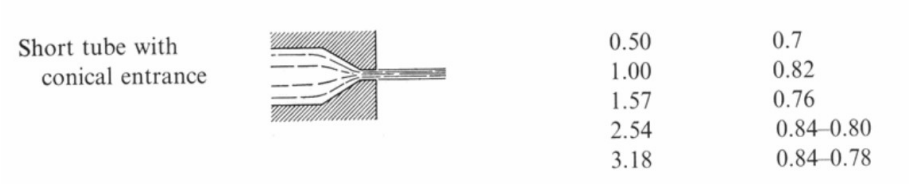

Figure 2.1: Injector scheme and data

Pressure losses due to the injection are considered to be a percentage of the p_c:

$$\Delta p_{inj} = 0.2 p_c = 4 \cdot 10^5 \, Pa \tag{2.10}$$

With the pressure losses, it is now possible to obtain a first approximation of the injection area by the inversion of the c_d formula:

$$A_{ox} = \frac{\dot{m}_{ox}}{c_d \sqrt{2 \Delta P_{inj} \rho_{ox}}} = 1.061 \cdot 10^{-6}\, m^2 \qquad A_{fu} = \frac{\dot{m}_{fu}}{c_d \sqrt{2 \Delta P_{inj} \rho_{fu}}} = 0.228 \cdot 10^{-6}\, m^2 \tag{2.11}$$

Once the area is known, the number of the injection holes needed can be determined approximating to the higher round number the result of Eq. 2.12:

$$N_{ox} = \frac{A_{ox}}{\pi \frac{d_{inj}^2}{4}} = 2 \qquad N_{fu} = \frac{A_{fu}}{\pi \frac{d_{inj}^2}{4}} = 1 \tag{2.12}$$

With these data available, the real area can be found multiplying the number of injectors by the area of the single injectors:

$$A_{ox,real} = N_{ox} \pi \frac{d_{inj}^2}{4} = 1.571 \cdot 10^{-6}\, m^2 \qquad A_{fu,real} = N_{fu} \pi \frac{d_{inj}^2}{4} = 0.785 \cdot 10^{-6}\, m^2 \tag{2.13}$$

The oxidizer flows exiting from the two injectors have been set to impinge with the fuel flow at an angle of 30°, guaranteeing a longitudinal complessive flow entering the chamber thanks to symmetry.

2.4 Pressure cascade

Different pressure losses can be individuated from the nozzle to the tanks, as reported in (Fig.2.2).

Setting the main geometrical quantities as reported below, each pressure loss can be separately discussed. The diameter of the feeding lines was set to 3 mm in order to have a moderate velocity of the propellants along the pipes in the order of 1-3 m/s. The length of the feeding lines (without considering the cooling jacket for the fuel) was set to 0.5 m, which is in the order of magnitude of the thruster length.

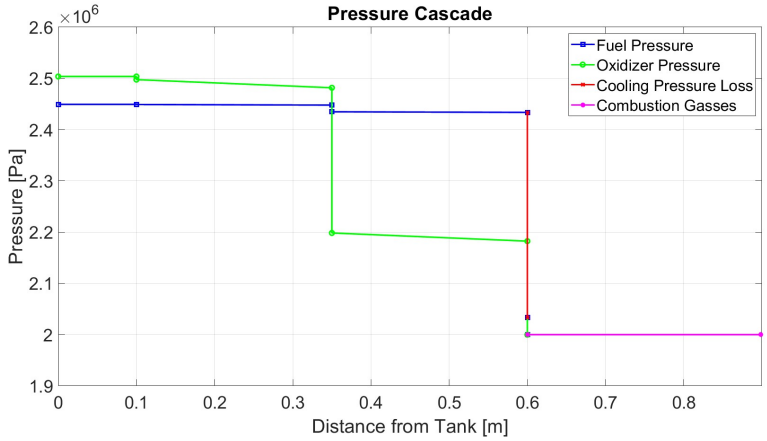

Figure 2.2: Pressure Cascade

2.4.1 Dynamic losses

The concentrated loss coefficients are determined as follows:

$$K_{ox,dyn} = \frac{8}{\rho_{H2O2}\pi^2 d_{feed}^4} = 7.443{\cdot}10^6 \frac{1}{kg \cdot m}, \; K_{fu,dyn} = \frac{8}{\rho_{RP-1}\pi^2 d_{feed}^4} = 1.235{\cdot}10^7 \frac{1}{kg \cdot m} \quad (2.14)$$

Now it is possible to compute the pressure losses due to the dynamic contribution:

$$\Delta P_{ox,dyn} = K_{ox,dyn}\dot{m}_{ox}^2 = 6057\ Pa \qquad \Delta P_{fu,dyn} = K_{fu,dyn}\dot{m}_{fu}^2 = 279.26\ Pa \quad (2.15)$$

2.4.2 Feeding line losses

In order to compute the equivalent concentrated loss coefficient, MATLAB function `feedloss` further described in Appendix 4.2 has been developed. Function inputs are: the mass flow rates, the density, the viscosity, the diameter and the length. At the start of the engine firing (nominal condition) the values of the losses are:

$$K_{ox,pipe} = 3.915 \cdot 10^7 \frac{1}{kg \cdot m} \qquad K_{fu,pipe} = 1.0315 \cdot 10^8 \frac{1}{kg \cdot m} \quad (2.16)$$

$$\Delta P_{ox,pipe} = K_{ox,pipe}\dot{m}_{ox}^2 = 31.858 \cdot 10^3\ Pa \qquad \Delta P_{fu,pipe} = K_{fu,pipe}\dot{m}_{fu}^2 = 2.332 \cdot 10^3\ Pa \quad (2.17)$$

2.4.3 Valve losses

For each pipe line one check valve and one latch valve have been selected. The nominal values needed to compute the pressure losses are reported in Appendix 4.4, Tab.4.4.
Consequently, the concentrated loss coefficients, which consider both the latch and the check valves, are:

$$K_{ox,valve} = 3.482 \cdot 10^8 \frac{1}{kg \cdot m} \qquad K_{fu,valve} = 5.779 \cdot 10^8 \frac{1}{kg \cdot m} \tag{2.18}$$

The pressure losses can be calculated as:

$$\Delta P_{ox,valve} = K_{ox,valve}\dot{m}_{ox}^2 = 2.833 \cdot 10^5\ Pa \qquad \Delta P_{fu,valve} = K_{fu,valve}\dot{m}_{fu}^2 = 0.131 \cdot 10^5\ Pa \tag{2.19}$$

2.4.4 Injection losses

The concentrated loss coefficients for the injectors are determined using:

$$K_{ox,inj} = \frac{1}{2\rho_{H2O2}(A_{ox,real}C_d)^2} = 2.2416 \cdot 10^8 \frac{1}{kg \cdot m} \tag{2.20}$$

$$K_{fu,inj} = \frac{1}{2\rho_{RP-1}(A_{fu,real}C_d)^2} = 1.4883 \cdot 10^9 \frac{1}{kg \cdot m} \tag{2.21}$$

Once the concentrated loss coefficients are computed, the pressure drops are now simply determined by:

$$\Delta P_{ox,inj} = K_{ox,inj}\dot{m}_{ox}^2 = 1.824 \cdot 10^5\ Pa \qquad \Delta P_{fu,inj} = K_{fu,inj}\dot{m}_{fu}^2 = 0.336 \cdot 10^5\ Pa \tag{2.22}$$

2.4.5 Cooling losses

Cooling losses are considered proportional to the combustion chamber pressure during the entire firing and are modelled as:

$$\Delta P_{cool} = 0.2P_c = 4 \cdot 10^5\ Pa \tag{2.23}$$

2.4.6 Tanks pressures

Now that all pressure losses for the nominal condition have been determined the initial tank pressures can be found:

$$P_{ox_i} = P_c + \Delta P_{ox,dyn} + \Delta P_{ox,pipe} + \Delta P_{ox,valve} + \Delta P_{ox,inj} = 2.504 \cdot 10^6\ Pa \tag{2.24}$$

$$P_{fu_i} = P_c + \Delta P_{fu,dyn} + \Delta P_{fu,pipe} + \Delta P_{fu,valve} + \Delta P_{fu,inj} + \Delta P_{cool} = 2.449 \cdot 10^6\ Pa \tag{2.25}$$

2.5 Tanks sizing

AISI 316 Stainless Steel is chosen as the tank material. A requested burning time t_b of 100 s yields the following on-board propellant masses and volumes.

$$M_{\text{ox}} = \dot{m}_{ox}\ t_b = 2.853\ kg \qquad M_f = \dot{m}_{fu}\ t_b = 0.475\ kg$$

$$V_{ox} = \frac{M_{ox}}{\rho_{ox}} = 2.122 \cdot 10^{-3}\ m^3 \qquad V_f = \frac{M_f}{\rho_f} = 0.587 \cdot 10^{-3}\ m^3$$

The pressurizing gas selected for both tanks is Helium (He) with the same temperature of the propellant couple (298.15 K): being a noble inert gas, it is characterized by low reactivity and represents a typical solution for LRE blow-down systems. Initial and final pressures of the two tanks are listed in the table below. Final pressures equal to 60% of the initial pressures have been selected through a trial and error method, in order to guarantee the requirements fulfillment.

Table 2.4: Sizing of the oxidizer and fuel tanks

	Oxidizer Tank	Fuel Tank
Initial Pressure $p_i[bar]$	25.037	24.493
Final Pressure $p_f[bar]$	15.022	14.696
Volume of the tank $[dm^3]$	5.3046	1.4674
Mass of the tank $[kg]$	0.550	0.150

2.6 Performance Analysis

In order to ensure that the nominal design respects the requirements presented by the company, a MATLAB algorithm to simulate the time evolution of the engine has been developed. Through a time discretization, at each time step, the oxidizer and fuel mass contained in the respective tanks are updated, with corresponding isothermal expansion of the loaded gas and reduction of the tank pressures, while the pressure cascade equations are numerically solved to determine the updated mass flow rates.
The specifics are presented in Appendix 4.5, while graphical results are shown in Fig. 2.3.

Figure 2.3: Trend of $\mathscr{F}$, I_s, p_c, T_c, O/F and $\dot{m}_p$ as function of the burning time

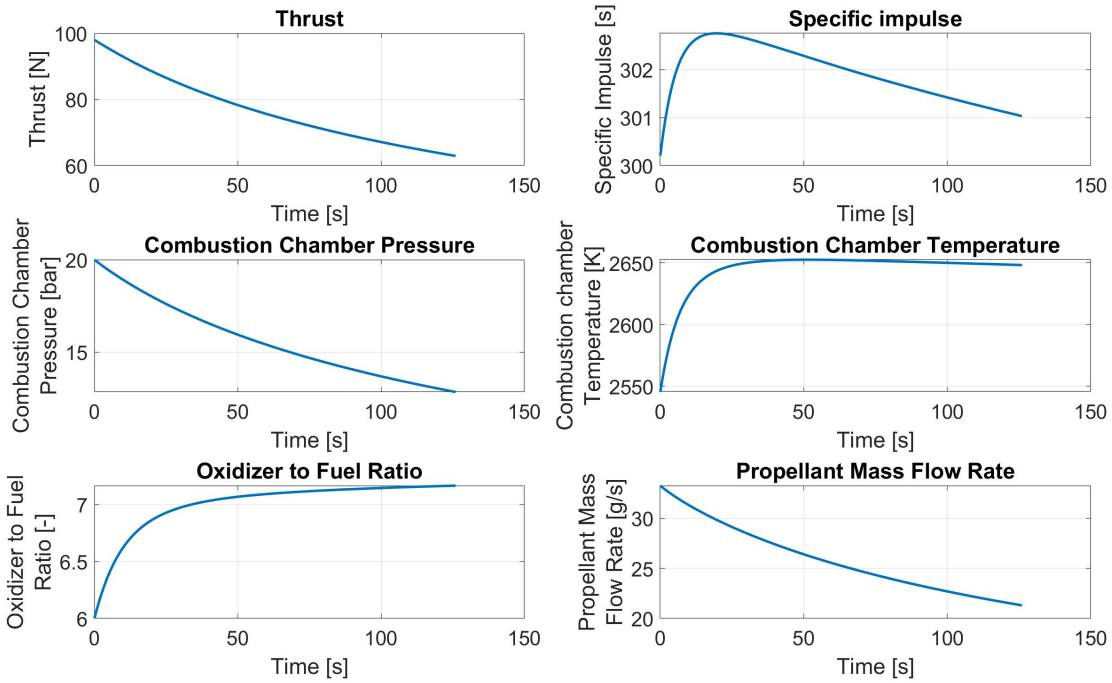

From the $\mathscr{F}$ chart, it is clear how the requirements on its decay and on the total firing time are satisfied. The I_s chart shows an expected peak delay of operations, which partially counters the reduction of the thrust due to the decay of the p_c. This is due to the choice of an initial sub-optimal O/F, which evolves towards more efficient O/F mixtures.

Chapter 3

Monte Carlo Analysis

3.1 Uncertainties Selection

The most relevant uncertainties in a liquid rocket engine are related either to the manufacturing side or the thermodynamic side.
From a manufacturing point of view the parameters to be taken into account are correlated to the additive manufacturing technique that has changing precision depending on the size of the part under construction; for larger parts the uncertainty is about 0.2% of the characteristic dimension [9], instead for the smaller parts the uncertainty is connected to the precision of the laser beam that is fixed and equal to 20-50 μm[9].
On the thermodynamic side there are multiple uncertainties that could be considered, for example: loaded masses, tank pressures, chamber pressure, flame temperature, mass flow rates and characteristic velocities. Considering that the thermodynamic uncertainties are easier to compensate during the experimental session and that they are affected by the manufacturing techniques but not *vice versa*, the most critical aspect is that of the additive manufacturing so the chosen uncertainties are correlated to the injection orifices diameter and the throat diameter.
For the injection orifices diameter, the uncertainty is connected to the additive manufacturing process: the hypothesis is that the tool has an intrinsic uncertainty which affects each hole in the same way. Same considerations can be done for the throat diameter, but, since the construction process is different, they are evaluated separately. For both, the selected maximum value of uncertainty is 50 μm.

3.2 Graphical Results

The chosen uncertainties are propagated through a Gaussian distribution since they were defined as of aleatory type, the results are populations of N values extracted from the respective distributions for each variable; then these values are combined together to obtain N^2 couples of random values, with N being the number of samples equal to 100.
For each couple the thrusts were used to compute for each iteration the cumulative mean value and the cumulative standard deviation of the thrust until that iteration.
It is important to underline how this evaluation has been done at the initial nominal condition. The obtained results for the thrust show a convergence to the value of 97.7661 N with an uncertainty of 1.81726 N with respect to the nominal value of 100 N (Fig.3.1).

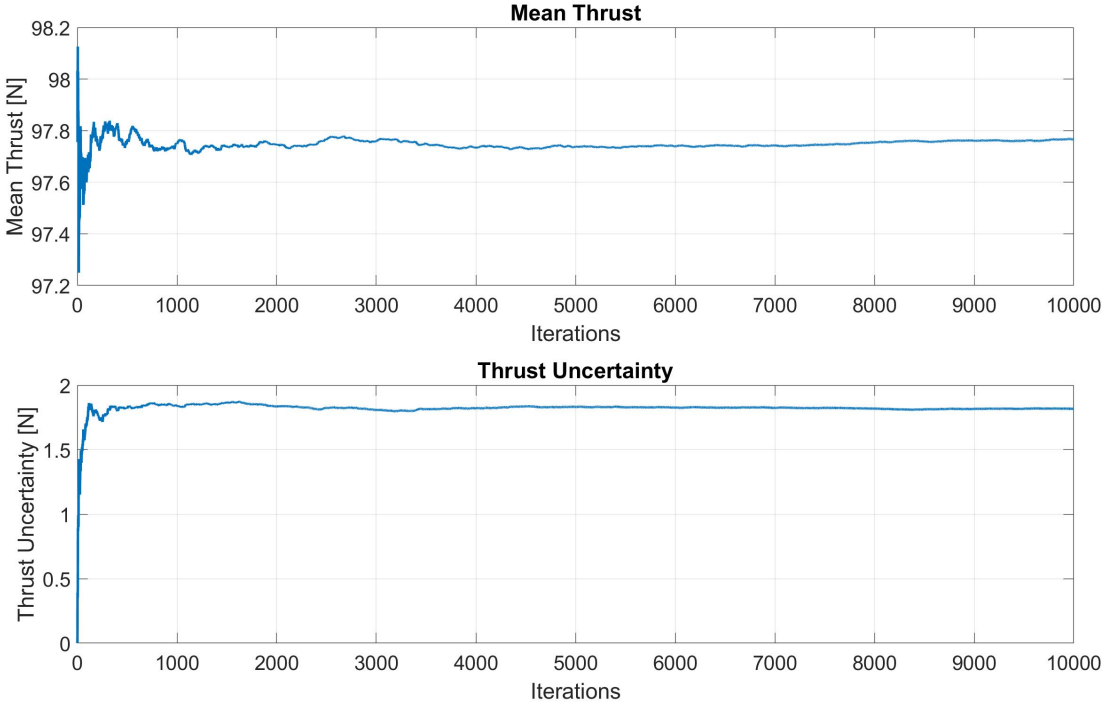

Figure 3.1: Nominal thrust and uncertainty

Moreover, computing the specific impulse and the combustion chamber pressure, the obtained results converge; in particular, the specific impulse converges to a mean value of 300.208 s with an uncertainty of 0.02628 s and the combustion chamber pressure converges to $2.00022 \cdot 10^6\ Pa$, with uncertainty $3.4735 \cdot 10^4\ Pa$ with respect to a nominal value of $2 \cdot 10^6\ Pa$ (Fig.3.2, Fig.3.3).

3.3 Qualitative Analysis for a 10 N and 1000 N Thrust Engine

For a smaller engine, due to a similar number of orifices, the uncertainty on the injection orificies diameter is not expected to produce particular variations. On the contrary, due to the reduction of the throat area, it is expected for the uncertainty to become far more relevant due to reduction in size of the throat diameter and subsequent increase of the relative error.
The opposite can be said about the 1000 N engine: due to the greater dimensions, small variations in the geometrical parameters are expected to have lower effects on the performances. As a matter of fact, for a larger motor a greater number of orifices is expected and, assuming each orifice having a different variation from the nominal value, an overall counter-balancing of the uncertainty effects on the total injection area is expected.
This behaviour is mostly due to the fact that the uncertainties of additive manufacturing are fixed independently on the dimension of the engine, so the smaller the engine is, the higher they are in percentage.

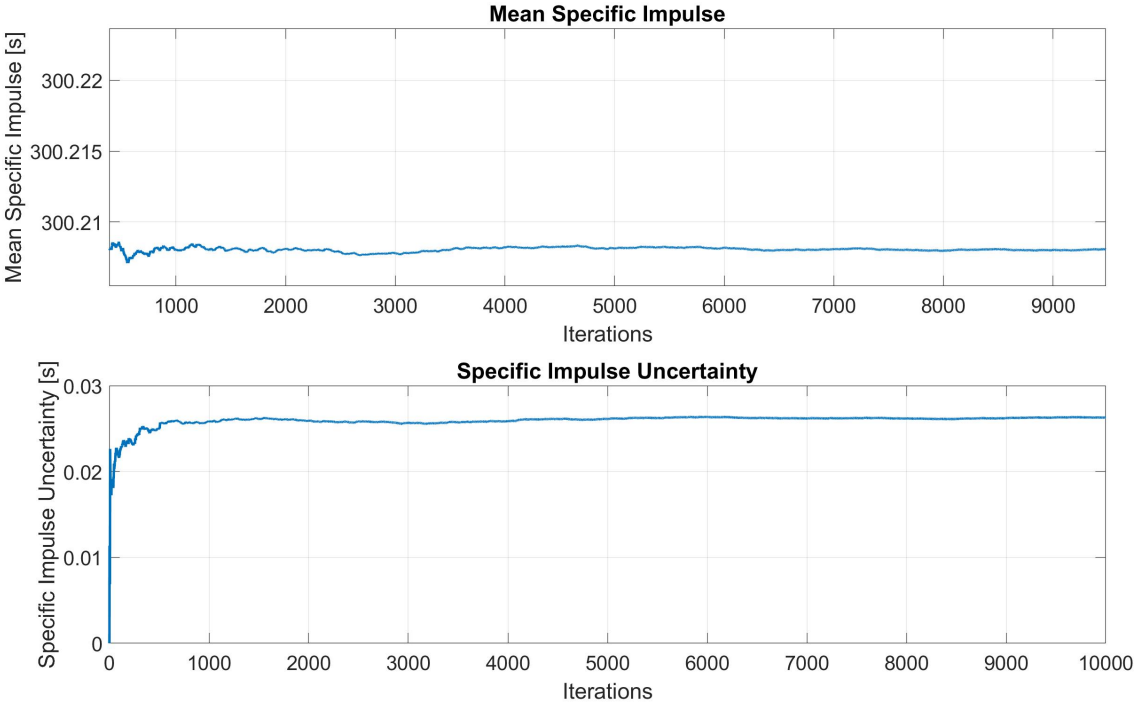

Figure 3.2: Nominal specific impulse and uncertainty

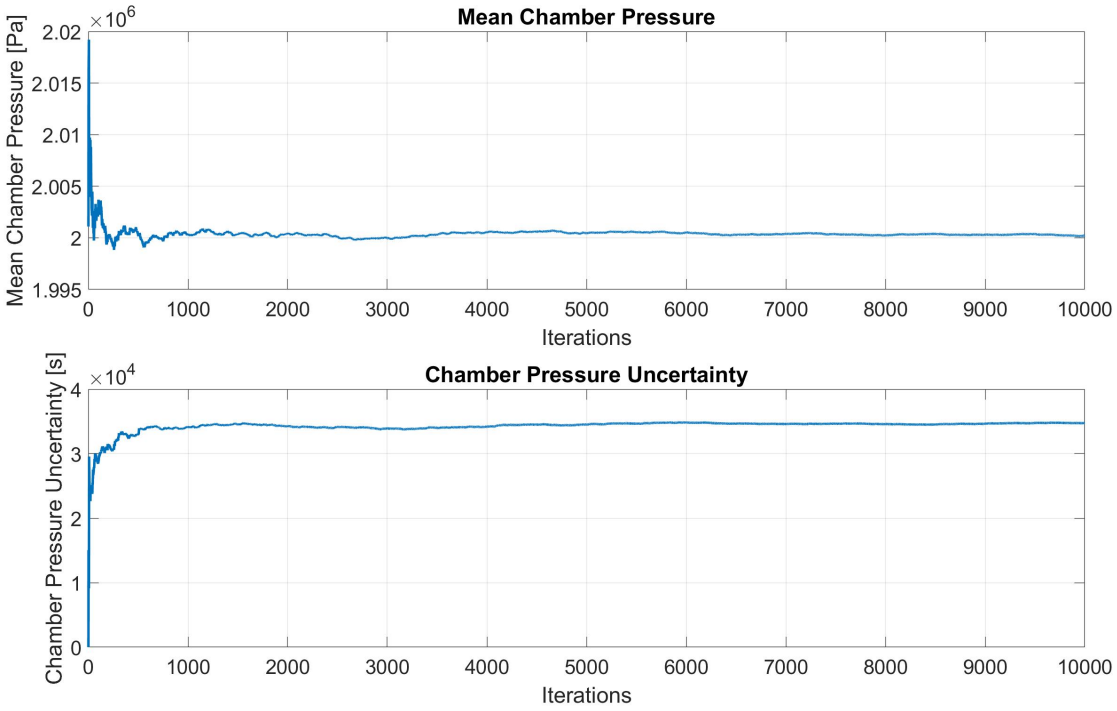

Figure 3.3: Nominal chamber pressure and uncertainty

Bibliography

[1] Notes from Space Propulsion Course held by Professor Maggi Filippo, Politecnico di Milano, 2022

[2] Henry Gary N., Humble Ronald W., Larson Wiley J., "Space Propulsion Analysis and Design", McGraw-Hill, 1995

[3] Huzel Dieter K., Huang David H., "Modern Engineering for Design of Liquid-Propellant Rocket Engines", American Institute of Aeronautics Revised, 1992

[4] Sutton George P., Biblarz Oscar "Rocket propulsion Elements", John Wiley Sonc Inc., 2010

[5] Terracciano A., Carapellese S., Bianchi G., Liuzzi D., Rudnykh M., Del Brusco F., "Additive Layer Manufacturing Technology in AVIO Injector Head Design", 7^{th} *European Conference for Aeronautics and Space Sciences (EUCASS)*, Colleferro (RM), 2017

[6] DebRoy T., Wei H.L., Zuback J.S., Mukherjee T., Elmer J.W., Milewski J.O., Beese A.M., Wilson-Heid A., De A., Zhang W., "Additive Manufacturing of Metallic Components - Process, Structure and Properties", Elsevier, 2017

[7] Singh Jagmit, Zerpa Luis E., Partington Benjamin, Gamboa Jose, "Effect of nozzle geometry on critical-subcritical flow transitions", Colorado School of Mines, 2018

[8] `https://www.prodways.com/wp-content/uploads/2021/12/P1000X_SLS_MACHINE.pdf`

[9] `https://www.prodways.com/wp-content/uploads/2020/07/in718_en.pdf`

[10] `https://www.specialmetals.com/documents/technical-bulletins/inconel/inconel-alloy-718.pdf`

[11] `https://www.vacco.com/images/uploads/pdfs/latch_valves_low_pressure.pdf`

[12] `https://www.scirp.org/journal/paperinformation.aspx?paperid=104531`

[13] `https://www.vacco.com/images/uploads/pdfs/check_valves.pdf`

[14] `https://propulsion-skrishnan.com/pdf/`

Chapter 4

Appendix

4.1 Nozzle and Combustion Chamber Geometry

Nozzle and combustion chamber geometries have been computed through the following equations:

- Nozzle design:

$$r_e = \sqrt{\frac{A_e}{\pi}} = 0.0258\,m \qquad r_t = \sqrt{\frac{A_t}{\pi}} = 0.0029\,m \tag{4.1}$$

$$L_{div} = \frac{r_e - r_t}{\tan\alpha} = 0.0854\,m \qquad L_{conv} = \frac{r_c - r_e}{\tan\beta} = 0.0049\,m \tag{4.2}$$

$$L_{tot} = L_{div} + L_{conv} = 0.0903\,m \tag{4.3}$$

- Combustion chamber design:

$$\varepsilon_c = \frac{A_c}{A_t} = \frac{1}{M_c}\left[\left(\frac{2}{\gamma+1}\right)\left(1 + \frac{\gamma-1}{2}M_c^2\right)\right]^{\frac{\gamma+1}{2\gamma-1}} = 5.9607 \tag{4.4}$$

$$A_c = \frac{\varepsilon_c}{A_t} = 1.552 \cdot 10^{-4}\,m^2 \qquad r_c = \sqrt{\frac{A_c}{\pi}} = 0.0070\,m \tag{4.5}$$

$$V_c = L^* A_t = 4.63 \cdot 10^{-5}\,m^3 \qquad L_c = \frac{V_c}{A_c} = 0.2983\,m \tag{4.6}$$

4.2 Feeding Lines' Losses Coefficent Computation

$$K = feedloss(\dot{m}_p, \rho_p, \mu_p, d_{feed}, L_{feed}) \tag{4.7}$$

Given an absolute roughness of AISI 316 Stainless Steel (taken from EUROBINOX Valves Datasheet) of $\epsilon = 0.8 \cdot 10^{-6}$, and the Reynolds number relative to the pipes' flow, it is possible to

compute the Darcy factor f. Then, the feeding lines' losses coefficient can be computed through a MATLAB function as[1]:

$$K = \frac{8 f L_{feed}}{\pi^2 \rho_p d_{feed}^5} \tag{4.8}$$

Darcy factor is computed using the laminar flow and the Colebrook equation:

$$\begin{cases} f = \frac{64}{Re} & if \;\; Re < 2000 \\ \frac{1}{\sqrt{f}} = -0.869 \cdot log(\frac{\epsilon}{3.7 \cdot D} + \frac{2.523}{Re \cdot \sqrt{f}}) & if \;\; Re > 2000 \end{cases}$$

Although for Reynolds numbers between 2000 and 4000 the flow enters the critical regime which is not well understood. For simplicity reasons $Re = 2000$ has been selected as a transition value between laminar and turbulent regimes.

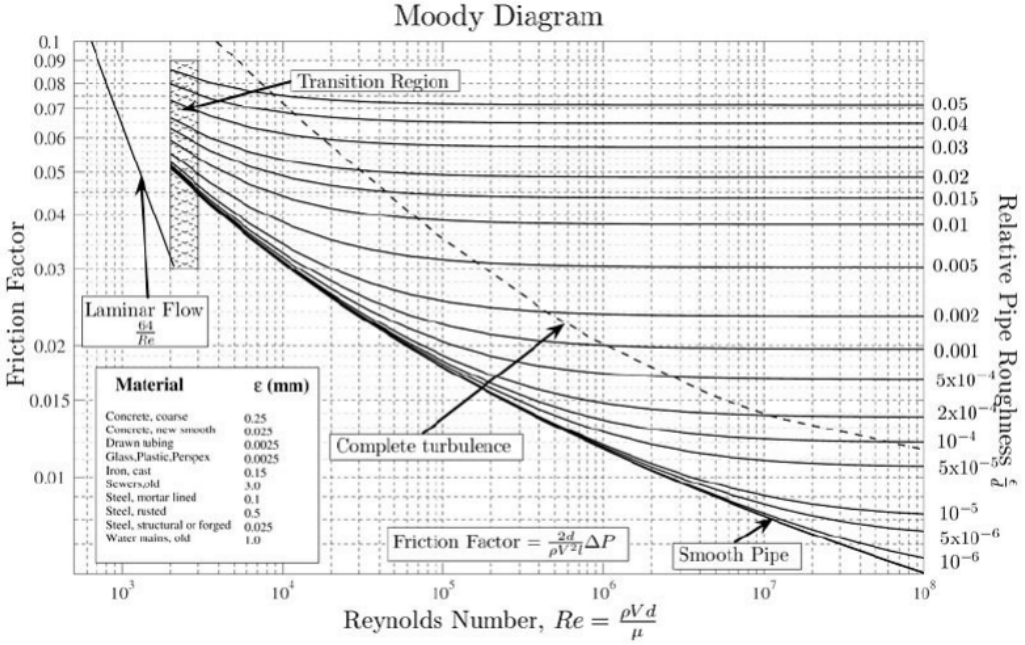

Figure 4.1: Moody Diagram for cross-check of f and Re values

4.3 Displacement Thickness Loss Computation

$$\lambda = disthick(p_c, T_c, \gamma, R, A_t, \mu_t) \tag{4.9}$$

In order to obtain the displacement thickness loss coefficient, it is required to firstly calculate the modified Reynolds number:

$$Re' = \sqrt{\frac{r_t}{r_{curv}}} Re_t \tag{4.10}$$

where r_t is the throat radius, while r_{curv} is the curvature radius taken from [7] as equal to 0.382. Then, by a MATLAB function:

$$\lambda = 1 - \left(\frac{\gamma+1}{2}\right)^{\frac{3}{4}} \left[3.266 - \frac{2.128}{\gamma+1}\right] \frac{1}{\sqrt{Re'}} + 0.9428 \frac{(\gamma-1)(\gamma+2)}{\sqrt{\gamma+1}} \frac{1}{Re'} \tag{4.11}$$

[1] All the quantities have to be referred to fuel or oxidizer depending on the analysis desired

4.4 Valves Pressure Drop

The propulsion system proposed in this paper utilizes two types of valves: a low pressure propellant latch valve and a low pressure check valve. The mass flow rates and the pressure drops are provided by VACCO Industries Datasheets ([11, 13]):

Table 4.1: VACCO Space Products Datasheet for valves

Valve Type	Valve Code	Mass Flow Rate $[kg/s]$	Pressure Drop $[Pa]$	Diameter $[m]$
Latch Valve	V1E10406-02	$1.30{\cdot}10^{-3}$	$3.4474 \cdot 10^{4}$	0.0063
Check Valve	V0D10840-01	$1.56 \cdot 10^{-4}$	$2.7579 \cdot 10^{4}$	0.0063

Having the actual radius of the valve it is possible to determine the relative area with:

$$A_{ref} = \pi \frac{d_{ref}^2}{4} = 3.1669 \cdot 10^{-5}\ m^2 \tag{4.12}$$

With the area, the pressure drop and the fluid density, the orifice pressure drop of the latch and the check valves can be determined [2]:

$$C_{d,check} = \frac{\dot{m}_{ref}}{A_{ref}\sqrt{2\rho\Delta P}} = 0.0499 \quad C_{d,latch} = \frac{\dot{m}_{ref2}}{A_{ref}\sqrt{2\rho_{He}\Delta P_2}} = 0.0431 \tag{4.13}$$

Now the concentrated loss coefficient for each valve type is found:

$$K_{ox,check} = \frac{1}{2\rho_{ox}(A_{ref}C_{d,check})^2} = 1.487 \cdot 10^{8}\ \frac{1}{kg \cdot m} \tag{4.14}$$

$$K_{fu,check} = \frac{1}{2\rho_{fu}(A_{ref}C_{d,check})^2} = 2.469 \cdot 10^{8}\ \frac{1}{kg \cdot m} \tag{4.15}$$

$$K_{ox,latch} = \frac{1}{2\rho_{ox}(A_{ref}C_{d,latch})^2} = 1.994 \cdot 10^{8}\ \frac{1}{kg \cdot m} \tag{4.16}$$

$$K_{fu,latch} = \frac{1}{2\rho_{fu}(A_{ref}C_{d,latch})^2} = 3.309 \cdot 10^{8}\ \frac{1}{kg \cdot m} \tag{4.17}$$

Then the total concentrated loss coefficient can be determined:

$$K_{ox,valve} = K_{ox,check} + K_{ox,latch} = 3.482 \cdot 10^{8}\ \frac{1}{kg \cdot m} \tag{4.18}$$

$$K_{fu,valve} = K_{fu,check} + K_{fu,latch} = 5.779 \cdot 10^{8}\ \frac{1}{kg \cdot m} \tag{4.19}$$

Finally the valve pressure drop can be computed:

$$\Delta P_{ox,valve} = K_{ox,valve} m_{ox}^2 = 2.833 \cdot 10^{5}\ Pa \tag{4.20}$$

[2] In this case the densities are referred to water ($\rho = 1000 kg/m^3$) and Helium ($\rho_{He} = 0.1785 kg/m^3$)

$$\Delta P_{fu,valve} = K_{fu,valve} m_{fu}^2 = 13063\ Pa \tag{4.21}$$

4.5 Model for Firing Simulation

The algorithm for evaluating the evolution of the engine is presented below:

1. The initial mass fluxes of oxidizer and fuel and chamber pressure at time $t = 0$ are employed to initialize the procedure. The time is increased of a timestep Δt;

2. The values of $\dot{m}_{ox}$, $\dot{m}_{fu}$ and p_c of the previous time steps are employed to interpolate the chamber tempertaure T_c, the specific gas constant R and the specific heat ratio γ from the CEA code datasheet;

3. The values of the characteristic velocity C^* and of the thrust coefficient c_F (considering the losses due to divergence and displacement thickness) are computed, as the thrust and the specific impulse;

4. The mass of the oxidizer and of the fuel in the respective tanks are reduced of an amount $\dot{m}_{ox}\Delta t$ and $\dot{m}_{fu}\Delta t$. The new values of the tank pressures (due to gas expansion);

5. The pressure cascade equations

$$\begin{cases} p_{ox,T} = (\dot{m}_{ox} + \dot{m}_{fu})\frac{c^*}{A_t} + K_{ox}(\dot{m}_{ox})\dot{m}_{ox}^2 \\ p_{fu,T} = (\dot{m}_{ox} + \dot{m}_{fu})\frac{c^*}{A_t} + K_{fu}(\dot{m}_{fu})\dot{m}_{fu}^2 \end{cases} \tag{4.22}$$

   are solved numerically to compute the new values of $\dot{m}_{ox}$ and $\dot{m}_{fu}$. The hydraulic resistances $K_{ox}(\dot{m}_{ox})$ and $K_{fu}(\dot{m}_{fu})$ are functions of the respective mass fluxes due to the dependance of the line hydraulic resistance from the Darcy factor, function of the Reynolds number which depends on the velocity/mass flux;

6. Increase the time of a time step Δt and restart from point 2, until M_{ox} and M_{fu} becomes zero or negative, condition which corresponds to complete spillage of fuel or oxidizer.

The complete code is reported in the following pages.

```
function [F_vec,Is_vec,OF_vec,Pc_vec,mox_vec,mfu_vec,Tc_vec,it,T_b,broken] = ...
    MODEL_BE(M_ox,M_fu,m_ox,m_fu,P_c,d_t,...
    PV_ox,PV_fu,V_oxt,V_fut,...
    d_inj,C_d,N_ox,N_fu,d_feed,L_feed,dt)

% INPUT
%  M_ox     Oxidizer mass in the tank [kg]
%  M_fu     Fuel mass in the tank [kg]
%  m_ox     Oxidizer mass flow rate [kg/s]
%  m_fu     Fuel mass flow rate [kg/s]
%  P_c      Chamber pressure [Pa]
%  d_t      Throat diameter [m]
%  PV_ox    Oxidizer tank gas isoterm constant (PV = const) [J]
%  PV_fu    Fuel tank gas isoterm constant (PV = const) [J]
%  V_oxt    Oxidizer tank volume (PV = const) [m^3]
%  V_fut    Fuel tank volume (PV = const) [m^3]
%  d_inj    Injectors diameter volume (PV = const) [m]
%  C_d      Injectors discharge coefficient [-]
%  N_ox     Numbers of injectors for oxidizer [-]
%  N_fu     Numbers of injectors for fuel [-]
%  d_feed   Diameter of feeding lines [m]
%  L_feed   Length of feeding lines [m]
%  dt       Time-step [m]
%
% OUTPUT
%  F_vec    Vector of thrusts at each time-step [N]
%  Is_vec   Vector of specific impulses at each time-step    [s]
%  OF_vec   Vector of specific          O/F ratios at each time-step [-]
%  Pc_vec   Vector of chamber pressures at each time-step [Pa]
%  mox_vec  Vector of oxidizer mass flow rates at each time-step [kg/s]
%  mfu_vec  Vector of fuel mass flow rates at each time-step [kg/s]
%  Tc_vec   Vector of chamber temperatures at each time-step [K]
%  it       Number of iterations [-]
%  T_b      Burning time [s]
%  broken   Output equaling "1" if the values of O/F and P_c
%           goes outside the domain of interpolation, else equaling "0"
%

eps = 80;

% Density of oxidizer [kg/s]
rho_H2O2 = 1414;
rho_H2O = 1000;
rho_ox = 100/(87.5/rho_H2O2 + 12.5/rho_H2O);

% Density of fuel [kg/s]
rho_fu = 810;

% Viscosity of oxidizer [Pa*s]
mu_ox = 1.249e-3;

% Viscosity of fuel [Pa*s]
mu_fu = 1.95e-6*rho_fu;

% Ground Earth acceleration [m^2/s]
g_0 = 9.81;

% Divergence thrust loss [m/s]
lambda_div = 0.5*(1+cosd(15));
```

```
% CEA code matrices for interpolation
[T_mat,R_mat,k_mat,mu_mat,OF_int,OF_min,OF_max,Pc_int] = CEA_reader;

% Preallocation of output vectors
F_vec = zeros(1,1e3);
Is_vec = zeros(1,1e3);
OF_vec = zeros(1,1e3);
Pc_vec = zeros(1,1e3);
mox_vec = zeros(1,1e3);
mfu_vec = zeros(1,1e3);
Tc_vec = zeros(1,1e3);

% Dynamic concentrated hydraulic resistances [1/(m*kg)]
K_ox1 = 8/(rho_ox*pi^2*d_feed^4);
K_fu1 = 8/(rho_fu*pi^2*d_feed^4);

% Injectors concentrated hydraulic resistances [1/(m*kg)]
K_ox2 = 1/(2*rho_ox*(N_ox*pi*d_inj^2/4*C_d)^2);
K_fu2 = 1/(2*rho_fu*(N_fu*pi*d_inj^2/4*C_d)^2);

% Computations for latch valves
dP_ref = 5*0.0689476e5; m_ref = 0.025*0.453592; rho_ref = 1000;
d_ref = 0.25*25.4e-3; A_ref = pi*d_ref^2/4;
C_dlv = m_ref/(A_ref*sqrt(2*rho_ref*dP_ref));

% Latch valves concentrated hydraulic resistances [1/(m*kg)]
K_oxlv = 1/(2*rho_ox*(A_ref*C_dlv)^2);
K_fulv = 1/(2*rho_fu*(A_ref*C_dlv)^2);

% Computations for check valves
dP_ref = 4*0.0689476e5; q_ref = 1.87*0.00047; rho_ref = 0.1785;
m_ref = rho_ref*q_ref; d_ref = 0.25*25.4e-3; A_ref = pi*d_ref^2/4;
C_dcv = m_ref/(A_ref*sqrt(2*rho_ref*dP_ref));

% Check valves concentrated hydraulic resistances [1/(m*kg)]
K_oxcv = 1/(2*rho_ox*(A_ref*C_dcv)^2);
K_fucv = 1/(2*rho_fu*(A_ref*C_dcv)^2);

% Valves concentrated hydraulic resistances [1/(m*kg)]
K_ox3 = K_oxlv + K_oxcv;
K_fu3 = K_fulv + K_fucv;

% Constant concentrated hydraulic resistances [1/(m*kg)]
K_ox = K_ox1 + K_ox2 + K_ox3;
K_fu = K_fu1 + K_fu2 + K_fu3;

% Lines hydraulic resistances (function of mass flow rates) [1/(m*kg)]
K_oxf = @(m_ox) K_f(m_ox,rho_ox,mu_ox,d_feed,L_feed);
K_fuf = @(m_fu) K_f(m_fu,rho_fu,mu_fu,d_feed,L_feed);

% Throat area [m^2]
A_t = pi*d_t^2/4;

% Characteristic velocity [m/s]
c_star = P_c*A_t/(m_ox+m_fu);

% Options for numerical solver
options = optimoptions('fsolve','Display','off');
```

```
it = 0;
broken = 0;
while M_ox > 0 && M_fu > 0  % Stop cycle if stored oxidizer/fuel mass is
                            % completely spent

    % Update iteration
    it = it + 1;

    % Compute O/F ratio
    OF = m_ox/m_fu;

    % Save O/F ratio
    OF_vec(it) = OF;

    % Compute P_c
    P_c = (m_ox+m_fu)*c_star/A_t;

    % Save P_c
    Pc_vec(it) = P_c;

    % Interpolate T_c, R, k and mu_t (chamber temperature, specific gas
    % constant, specific heat ratio, viscosity in throat)
    T_c = interpn(OF_int,Pc_int,T_mat,OF,P_c,'cubic'); Tc_vec(it) = T_c;
    R = interpn(OF_int,Pc_int,R_mat,OF,P_c,'cubic');
    k = interpn(OF_int,Pc_int,k_mat,OF,P_c,'cubic');
    mu_t = interpn(OF_int,Pc_int,mu_mat,OF,P_c,'cubic');

    % Compute c*
    c_star = sqrt(R*T_c)/sqrt(k*(2/(k+1))^((k+1)/(k-1)));

    % Compute
    r_P = fzero(@(x) 1/eps - ((k+1)/2)^(1/(k-1))*x^(1/k)*sqrt((k+1)/(k-1)*(1-
    x^((k-1)/k))),[0 1e-2]);

    % Compute displacement thickness thrust loss
    lambda_DT = DT_loss(P_c,T_c,k,R,A_t,mu_t);

    % Compute thrust coefficient
    C_F = lambda_div*lambda_DT*sqrt(2*k^2/(k-1)*(2/(k+1))^((k+1)/(k-1))*(1-
    r_P^((k-1)/k))) + eps*r_P;

    % Compute thrust
    F = C_F*P_c*A_t;

    % Save thrust
    F_vec(it) = F;

    % Compute specific impulse
    I_s = c_star*C_F/g_0;

    % Save specific impulse
    Is_vec(it) = I_s;

    % Reduce oxidizer and fuel mass contained in the respective tanks
    M_ox = M_ox - m_ox*dt;
    M_fu = M_fu - m_fu*dt;

    % Compute new tank pressures through isoterm relation
```

```
    P_ox = PV_ox/(V_oxt - M_ox/rho_ox);
    P_fu = PV_fu/(V_fut - M_fu/rho_fu);

    % Numerically solve pressure cascade equations
    f = @(m_ox,m_fu) [
        (m_ox+m_fu)*c_star/A_t + (K_ox+K_oxf(m_ox))*m_ox^2 - P_ox
        1.2*(m_ox+m_fu)*c_star/A_t + (K_fu+K_fuf(m_fu))*m_fu^2 - P_fu
        ];
    X = fsolve(@(x) f(x(1),x(2)),[m_ox m_fu],options);

    % Set new mass flow rates
    m_ox = X(1);
    m_fu = X(2);

    % Save mass flow rates
    mox_vec(it) = m_ox;
    mfu_vec(it) = m_fu;
end

% Eliminate unused spaces from preallocated output vectors
F_vec = F_vec(1:it);
Is_vec = Is_vec(1:it);
OF_vec = OF_vec(1:it);
Pc_vec = Pc_vec(1:it);
mox_vec = mox_vec(1:it);
mfu_vec = mfu_vec(1:it);
Tc_vec = Tc_vec(1:it);

% Compute total burning time
T_b = (it-1)*dt;

end
```